Lab on a Chip

PAPER

View Article Online
View Journal | View Issue

Cite this: *Lab Chip*, 2025, **25**, 5379

Modular, open-sourced multiplexing for democratizing spatial omics

Nicholas Zhang,[abc] Zhou Fang,[ac] Priyam Kadakia,[ac] Jamie Guo,[ac] Dakshin Vijay,[ac] Manoj Thapa,[d] Samuel Dembowitz,[ac] Arash Grakoui[d] and Ahmet F. Coskun *[abc]

Spatial omics technologies have revolutionized the field of biology by enabling the visualization of biomolecules within their native tissue context. However, the high costs associated with proprietary instrumentation, specialized reagents, and complex workflows have limited the broad application of these techniques. In this study, we introduce Python-based robotic imaging and staining for modular spatial omics (PRISMS), an open-sourced, automated multiplexing pipeline compatible with several biospecimen targets and streamlined microscopy software tools. PRISMS utilizes a liquid handling robot with thermal control to enable the rapid and automated staining of RNA and protein samples. The modular sample holders and Python control facilitate high-throughput, single-molecule fluorescence imaging on widefield and confocal microscopes. We successfully demonstrated the versatility of PRISMS by imaging tissue slides and adherent cells. We demonstrate that PRISMS can be utilized to perform super-resolved imaging, such as super-resolution radial fluctuations (SRRF). PRISMS is a powerful tool that can be used to democratize spatial omics by providing researchers with an accessible, reproducible, and cost-effective solution for multiplex imaging. Specifically, PRISMS is an open-source, automated multiplexing pipeline for spatial omics, compatible with several sample types and Nikon NIS Elements Basic Research software, as well as Python-based biodevices. It performs high-throughput, single-molecule fluorescence imaging both on widefield and confocal microscopes, and can be used to perform super-resolved imaging, such as SRRF. Overall, PRISMS is a powerful tool that can be used to democratize spatial omics by providing researchers with an accessible, reproducible, and cost-effective solution for multiplex imaging. This open-source platform will enable researchers to push the boundaries of spatial biology and make groundbreaking discoveries.

Received 22nd March 2025,
Accepted 26th August 2025

DOI: 10.1039/d5lc00286a

rsc.li/loc

Introduction

Recent advances in spatial omics have necessitated the use of expensive reagents, long imaging durations, and computationally intensive computations with larger image datasets. Additionally, proprietary software to automate these laborious (and often cyclic) pipelines has further exacerbated these barriers to entry. As demonstrated in recent high-impact studies, these techniques reveal not only the spatial distribution of biomolecules but also the intricate interplay between different cell types within their native microenvironments. However, the broad application of spatial omics has been largely confined to well-resourced laboratories due to the high costs associated with proprietary instrumentation, specialized reagents, and complex workflows. The rising demand for high-resolution spatial data in fields ranging from cancer biology to neuroscience is accompanied by escalating operational costs and technical challenges. Conventional spatial omics methods often require significant investments in both hardware and consumables, creating barriers for smaller laboratories and limiting the pace of innovation. In contrast, open-sourced, democratized approaches have the potential to transform the landscape of spatial omics by providing accessible, reproducible, and cost-effective solutions. By leveraging community-driven innovations and automating key processes such as sample staining and imaging, researchers can standardize protocols, reduce variability, and ultimately accelerate discovery.

Thus, we introduce Python-based robotic imaging and staining for modular spatial omics (PRISMS), an open-sourced, automated multiplexing pipeline compatible with

[a] *Wallace H. Coulter Department of Biomedical Engineering, Georgia Institute of Technology and Emory University, Atlanta, GA, USA.*
E-mail: ahmet.coskun@bme.gatech.edu
[b] *Interdisciplinary Bioengineering Graduate Program, Georgia Institute of Technology, Atlanta, GA, USA*
[c] *Parker H. Petit Institute for Bioengineering and Bioscience, Georgia Institute of Technology, Atlanta, GA, USA*
[d] *Division of Microbiology and Immunology, Emory National Primate Research Center, Emory University, Atlanta, Georgia*

several sample types and Nikon NIS Elements Basic Research software to run a Nikon widefield TE-2000U fluorescence microscope. Our pipeline consists of an open-sourced Python (Jupyter notebook) that 1) writes command-level NIS Elements commands for custom image acquisition, 2) computes autofocus correction for Z drift, and 3) writes a Fiji/ImageJ macro to stitch overlapping images for large scan imaging. User input only involves a series of saved *ZYX* coordinates for a sample of interest with options to 1) capture individual fields of view (FOVs), 2) tile scan the entire area encompassing all selected coordinates, or 3) tile scan each FOV with a certain size (*e.g.*, 3 × 3 FOVs per coordinate). Furthermore, multiple Python notebooks can be "chained" together to image each sample (*e.g.*, 3 tissue slides) sequentially, thus increasing imaging throughput with no user input. Multiple sample formats are compatible with our 3D-printed multiplex mount (up to 3 tissue slides) and laser-cut acrylic holders (for coverslips), enabling successful cyclic imaging. Any well plate format is directly compatible with the Nikon widefield stage.

This custom pipeline is especially useful, for example, in super-resolved acquisitions such as super-resolution radial fluctuations (SRRF).[1] SRRF requires repeated (~100) frame imaging of single *Z* coordinates, which is not an option in typical imaging software. With our open-sourced pipeline, we enable custom repeated frame imaging combined with automated super-resolved reconstructions that can easily be run in Fiji/ImageJ once the Fiji macro is generated (Fig. 1).

Finally, our pipeline can also perform automated post-processing such as background subtraction, thresholding, and individual channel rendering for quick inspection of image quality. Such automated processing provides quick insight into single-cell statistics (Fig. 2) and general expression patterns among tissues when relevant. Here, we successfully demonstrate our pipeline on tissue slides, cells on coverslips, cells in 96 or 12-well plates, and cells in custom well formats.

Existing advances in computational biology have focused heavily on data mining to yield unique biological insights, *e.g.*, Xenium, MERSCOPE, Sopa, CosMX, MACSima, and Phenocycler.[2–7] While these technologies excel at uncovering spatial transcriptomic or proteomic relationships *via* segmentation, annotation, phenotyping, neighborhood analyses, *etc.*, their proprietary nature (except Sopa) requires high costs, custom software, and/or custom reagents (for acquisition). Furthermore, their "black box" characteristics leave little room for fine-tuning how data is acquired. In contrast, PRISMS is an open-source, customizable Python workflow for Nikon microscopes, capable of tailoring acquisition and analyses to fit a range of user needs. We successfully demonstrated PRISMS with cell imaging, stitched tissue scans, and SRRF enhancements, complete with cell segmentation, analyses, and quantification.

PRISMS offers a fundamentally new solution by providing an open-source, customizable Python workflow specifically for Nikon microscopes and Cephla spinning disk confocals. It enables tailoring acquisition and analyses to fit a range of user needs, unlike proprietary technologies that often have "black box" characteristics and limit fine-tuning. Compared to commercial spatial omics pipelines such as Visium, Xenium, CosMx, PhenoCycler, MERSCOPE, PRISMS offers user tuning at any step and does not restrict reagent use. For post-processing, PRISMS can perform automated repeated frame imaging for super-resolution radial fluctuations (SRRF) and generate Fiji macros for reconstructions, which are not always available in standard imaging software. Therefore, PRISMS offers a unique combination of open-source code, specific integration with Nikon microscopes, modular hardware, and automation of key spatial omics tasks, differentiating it from existing products.

The vast majority of open source workflows are designed for processing, not acquisition. For example, Spacemake, built using Snakemake and Python, is inherently modular, allowing users to configure and extend the pipeline for various spatial transcriptomics technologies. It can process and analyze multiple samples in parallel, even from different experimental methods. Modules cover steps from raw sequencing data to downstream analysis reports, including sample merging and integration with single-cell data.[8] As a Snakemake-based workflow, it offers robust automation of processing steps once configured. It aims for reproducible data processing and automatically generated analysis reports. Another tool designed with a clean, modular Python structure, called ST Pipeline, breaks down the processing of spatial transcriptomics data into distinct steps, including quality filtering, mapping, and generation of spatial count matrices.[9] It features a command-line interface that allows for efficient and automated execution of these steps, facilitating batch processing of samples. Likewise, Squidpy, built on top of Scanpy and AnnData, provides a framework of tools for spatial omics analysis. Its functions are organized into modules for different analysis tasks like image processing, spatial statistics, and visualization, allowing users to construct custom analysis workflows.[10] While highly interactive, Squidpy's Python-based nature allows for scripting and automation of complex analysis sequences. Another tool, Panpipes, consists of a set of computational workflows designed for multimodal single-cell and spatial transcriptomic analyses.[11] It incorporates widely-used Python-based tools and is structured into distinct workflows for ingestion, preprocessing, integration, clustering, and visualization. It is designed to automate these analysis stages at scale, enabling reliable and customizable processing of individual and integrated modalities. SPArrOW is another tool described as a flexible, modular, and scalable pipeline. Its basic building blocks are tightly integrated and can process spatial omics datasets in a parallelized fashion. It allows sample-specific pipeline optimization through tunable parameters.[12] While offering interactive visualization and human-in-the-loop optimization, its workflow structure supports automated processing once parameters are set. Despite their computational advantages, all of these open-source tools cannot acquire data or fine-tune data acquisition.

Commercial solutions often provide end-to-end systems, from sample preparation and imaging to data analysis software. These platforms typically emphasize user-friendliness,

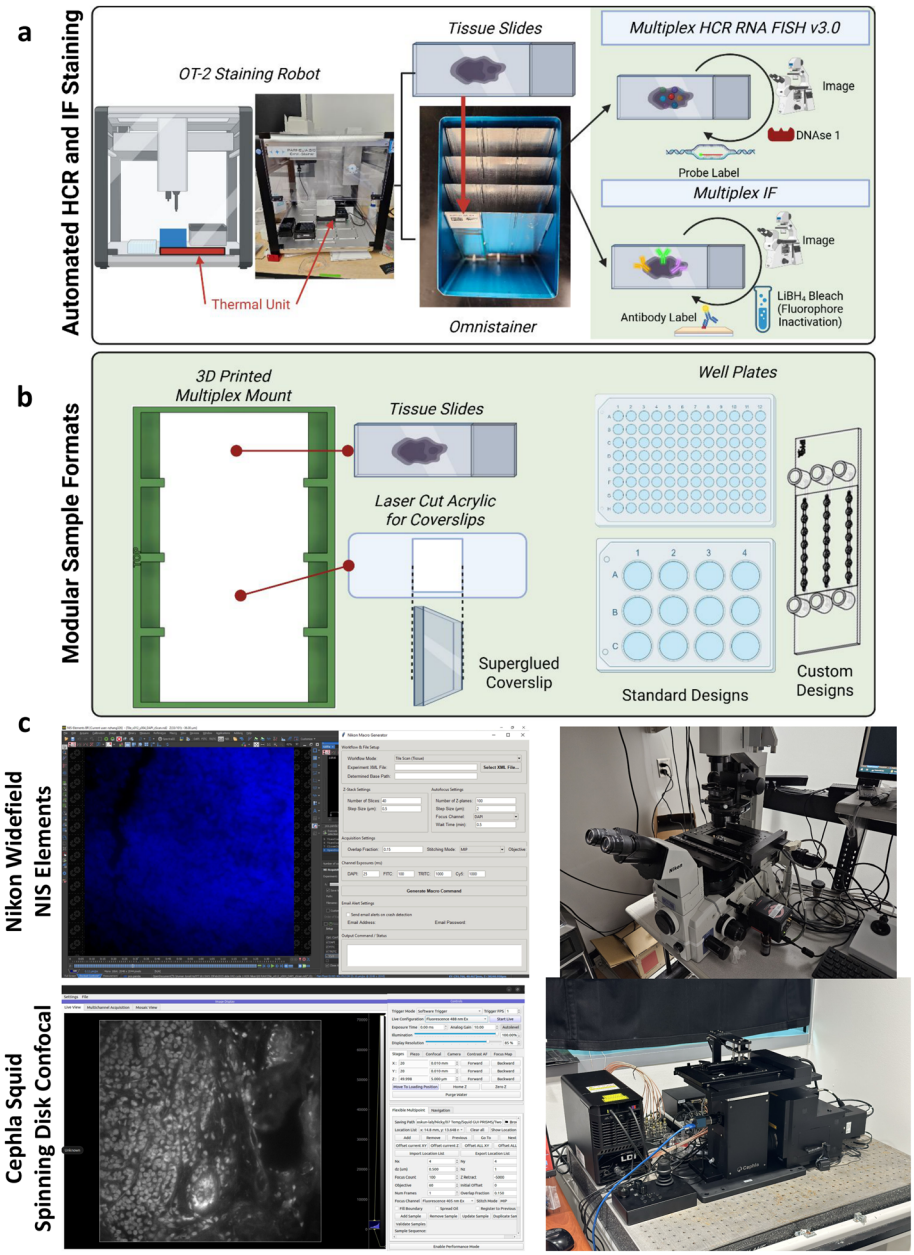

Fig. 1 Open-sourced PRISMS is compatible with a variety of sample formats, acquisition modes, and post-processing reconstructions. a) Rapid, multiplex staining with the OT-2 staining robot of up to 12 slides or coverslips contained in an Omnistainer (blue) in a single run. Temperature modules facilitate both HCR RNA and IF protein staining. Cyclic multiplexing is achieved by removing labeled fluorescence with DNAse I enzyme (RNA) or LiBH4 photobleaching (protein), followed by repeated staining and imaging. b) Modular sample formats allow imaging of various sample types. Examples include a custom 3D printed mount for up to 4 tissue slides (green). Laser-cut acrylic mounts can also substitute for each slide and hold a 22 × 22 mm or larger coverslip for cell samples. PRISMS will also work for prototypical, glass-bottom well plate formats: 96, 24, 12-well, *etc.* Additionally, custom chip designs, such as ones sold by Ibidi©, are also compatible. Created with **BioRender.com**. c) Representative images of imaging on both Nikon widefield (top) and Cephla© spinning disk confocal (bottom) setups. The left column illustrates the interactive GUI used to set up automated acquisition. The right column shows the true imaging setup.

robustness, and dedicated support, with varying degrees of disclosed modularity but strong automation. However, they suffer from high costs, strict reagent guidelines and sample formats, and a lack of acquisition customization. For example, the 10× Genomics Visium and Space Ranger is a set of analysis pipelines that process 10× Visium spatial gene expression data. While the internal workings are proprietary, it consists of distinct computational steps (*e.g.*, alignment, barcode/UMI processing, feature counting, and clustering). Space Ranger automates the entire process from FASTQ files to summary reports and data files for visualization (*e.g.*, Loupe Browser). The 10× Visium pipeline requires specific sample formats (*e.g.*, fresh, methanol-fixed, and cryopreserved samples) and lacks single-cell resolution, let alone any tunability during acquisition.

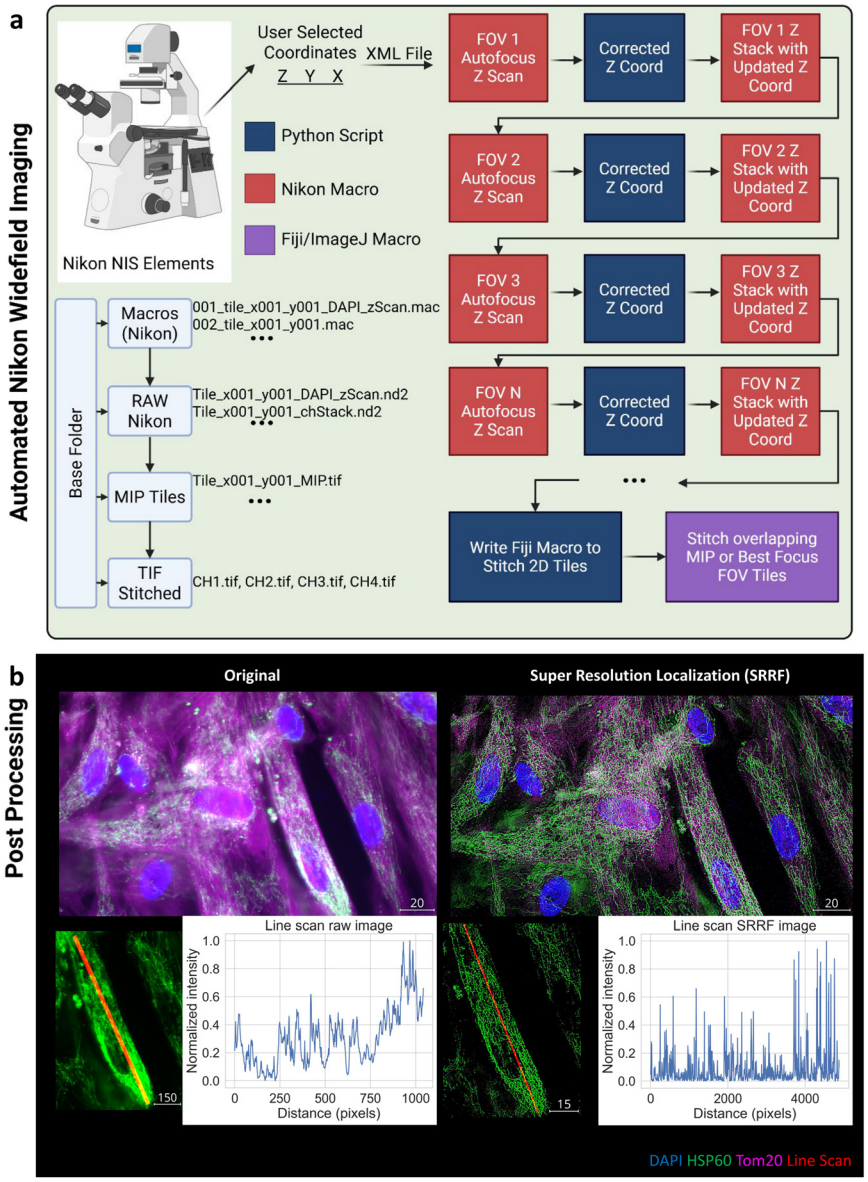

Fig. 2 PRISMS widefield imaging pipeline. a) Main PRISMS imaging widefield acquisition workflow. Samples can be scanned with Z stack and selected fluorescent channels for multiple fields of view (FOVs), contiguous FOVs for stitching, or a combination of both, in which each FOV comprises its contiguous scan, *e.g.*, 3 × 3 tiles. Regardless, each FOV is first Z-scanned on a focus channel, typically DAPI, paused for Python to compute the focus *Z* coordinate, updated in Nikon macros with the computed *Z* coordinate, and finally acquired with *Z* and channel filters. This process is repeated until all FOVs are acquired. If stitching a region defined by a boundary, Python will write a Fiji macro that can be run to stitch overlapping FOVs. Each segment of the workflow is colored by the respective programming language: Python/Jupyter (dark blue), Nikon (red), or Fiji (purple). For faster processing, tiles for stitching are computed in real time as images are acquired. Example folder structure for a single acquisition is shown in the bottom left diagram. Created with **BioRender.com**. b) PRISMS widefield post-processing enhancements with SRRF.[1] If repeated frames are acquired, PRISMS will write a Fiji macro to execute the open-source SRRF tool to reconstruct the super-resolved frames. The example shown is for umbilical cord-derived mesenchymal stem cells (UC-MSCs). Original 3D images, average of repeated Z frames, and super-resolved reconstructions are shown for the same region. Super-resolved labels include DAPI (blue), HSP60 (green), and Tom20 (green). Line scan quantifications from the red line are shown at the bottom, illustrating the more frequent, sharper peak intensity profiles in SRRF than in widefield across the same cell.

Another spatial omics platform, the NanoString GeoMx® Digital Spatial Profiler (DSP) & CosMx™ Spatial Molecular Imager (SMI) with AtoMx™ Spatial Informatics, involves integrated hardware and software. The AtoMx platform, being cloud-based, offers modular analysis applications for data from GeoMx and CosMx systems. The systems are designed for high-throughput, automated data acquisition, and streamlined data analysis through the AtoMx platform. Similarly, the Akoya Biosciences PhenoCycler® (formerly CODEX) and PhenoImager® HT (formerly Vectra Polaris) provide tools for high-plex tissue imaging. The analysis software (*e.g.*, inForm®, Proxima™) offers modules for image analysis, cell segmentation, and scoring. The platforms are designed for automated sequential imaging (PhenoCycler) and

high-throughput slide scanning (PhenoImager HT), with software facilitating automated image processing and data extraction. Higher plex spatial transcriptomic platforms such as Vizgen MERSCOPE™, based on multiplexed error-robust fluorescence *in situ* hybridization (MERFISH), contain modules for image processing, transcript decoding, and quality control.[13] The MERSCOPE instrument automates the fluidics, imaging, and primary data processing steps required for MERFISH. For higher-end imaging, Zeiss Microscopes and ZEN Software offer various modules for image acquisition, processing (*e.g.*, AI-powered segmentation with Cellpose integration), and analysis tailored to microscopy data, which is foundational for many spatial omics techniques. The software can automate complex imaging routines and analysis workflows, including 3D multiplexing. However, these tools suffer from very high costs, limited reagent selection, little to no acquisition customization, and difficult integration with custom parts. Hence, PRISMS offers a cost-effective solution with minimal proprietary components, modular parts, and potentially unlimited customizations by the end user.

Comparable, open-sourced solutions are fewer in number. For example, Open-ST offers open-sourced, subcellular spatial transcriptomics labeling of 2D and 3D samples using an adapted Illumina flow cell.[14,15] It enables cost-efficient whole-transcriptome analysis by repurposing Illumina flow cells as RNA capture areas. Open-ST has demonstrated the ability to identify cell populations, tissue heterogeneity, and biomarkers across various biological samples, including human tumors and mouse brain tissues. Open-ST also integrates computational tools to facilitate seamless data processing, from RNA capture to transcriptomic mapping. It employs an optimized pipeline for image segmentation and spatial transcriptomics integration, thereby reducing the need for manual intervention. The system is highly adaptable, allowing researchers to fine-tune segmentation, visualization, and computational analysis for different tissue types and experimental setups. The framework provides open-source software for customization, enabling 3D reconstruction and multimodal analysis of tissue samples. While Open-ST is more cost-efficient than many commercial alternatives, it requires specific resources that may not be readily available in every laboratory. The method leverages repurposed Illumina flow cells, a custom sequencing recipe, and even a 3D-printable cutting tool for controlled fragmentation. These custom tools and protocols necessitate a level of technical expertise and access to specialized sequencing platforms, such as the NovaSeq6000, which could limit broader adoption for some research groups. The method's ability to generate subcellular resolution and reconstruct 3D virtual tissue blocks introduces significant computational complexity. Processing, aligning, and integrating datasets across serial sections requires advanced algorithms and substantial computational resources. Although the reported registration accuracy is approximately 1 μm, even minor alignment errors can be critical when interpreting spatial relationships in densely packed or heterogeneous tissue regions. Furthermore, the size of each capture area is inherently limited by the sequenced area of the flow cell lane (maximum of approximately 6.3 × 89 mm), which may restrict the throughput when very large tissue sections need to be analyzed in one run.

One open-source, a single-molecule detection tool for live cell analysis, AiSIS, has been successfully deployed.[16] AiSIS is a fully automated imaging system that integrates advanced TIRF optics, deep learning, and robotics into a modular design to enable high-throughput live-cell analysis. The system automates key processes—including cell selection *via* deep learning, precise autofocusing based on iris image analysis, and consistent immersion-oil regulation—eliminating manual intervention and reducing variability while dramatically increasing processing speed by up to 10- to 100-fold. AiSIS was applied to image and track fluorescent epidermal growth factor receptors (EGFRs) across 1600 cells in a 96-well plate within a single day, demonstrating its ability to capture dynamic changes in receptor mobility in response to varying ligand concentrations. Quantitative analyses measured critical parameters such as diffusion coefficients, oligomer sizes, and half-maximal effective concentrations (EC_{50}), thereby validating the system's potential to transform single-molecule screening, cell signaling studies, and drug discovery. Despite its transformative automation of single-molecule imaging, AiSIS has several limitations. Its performance heavily relies on high-quality training data and precise calibration for deep-learning-based autofocus and cell selection, meaning that adjustments may be necessary for different cell types or imaging conditions. In practice, a small proportion of cells, such as those where fluorescent spots could not be reliably tracked, demonstrate that the system can still encounter issues with cellular heterogeneity and low signal intensity. Additionally, the technology is optimized for TIRF microscopy, and the specific hardware setup required (including expensive optics, robotic manipulators, and immersion oil management) may limit its adaptability to other imaging modalities or labs with restricted resources. A direct comparison of these spatial omics technologies with PRISMS is provided in Table S1.

While Pycro-Manager and Napari are also existing Python-based research microscope tools, they serve different purposes than PRISMS. Napari is a versatile image rendering tool, providing quick and easy viewing of large microscopic images, including 3D rendering capabilities.[17] However, Napari does not directly possess microscopic data acquisition capabilities. Currently, PRISMS GUI also contains Napari viewing capabilities for quick viewing of sample images. On the other hand, Pycro-Manager is a robust open-source software that acts as a bridge between the extensive hardware support of μManager (written in Java and C++) and the powerful scientific computing ecosystem of Python.[17] It aims to provide a flexible and user-friendly programming interface for customized and reproducible microscope control. However, Pycro-Manager is a software library for microscope control, not an end-to-end application pipeline like PRISMS. Users must build their own specific applications and

workflows on top of it. Additionally, as a bridge between different programming languages and software (Python, Java, μManager), the initial setup and understanding of the software architecture might be complex for new users. While it can be integrated into larger workflows, Pycro-Manager's primary strength lies in data acquisition control rather than the full-spectrum automation of staining and post-processing seen in PRISMS.

Results and discussion

Liquid handling robot with thermal control enables multiplex HCR RNA FISH v3.0 and immunofluorescence with minimal reagent volumes

First, we implement a rapid, automated staining system using the OT-2 robot that is compatible with Opentrons technology (Fig. 1a). The sample holder can hold up to 12 slide samples. With the inclusion of the thermal module, following manual baking, dewaxing, and antigen retrieval, we successfully multiplexed RNA with Molecular Instruments' Hybridized Chain Reaction (HCR) v3.0 and protein with cyclic immunofluorescence (IF).[18,19] The thermal sheath minimizes evaporation loss, and we ensure temperatures are accurate after calibration (Fig. S1).

Modular sample formats and Python control facilitate open-sourced, high-throughput, single-molecule fluorescence imaging on widefield and confocal microscopes

For imaging, we 3D printed (*via* fused deposition modeling) a custom 4-slide holder (Fig. 1b). Additionally, our PRISMS workflow is compatible with well plates of varying sizes and custom Ibidi coverslips. For imaging, we operate similar workflows on Nikon widefield (NIS Elements BR©) and Cephla spinning disk confocal, which are both directed by Python scripts and a basic graphical user interface (GUI) (Fig. 1c, Tables S2 and S3). Nikon NIS Elements software is capable of performing advanced image acquisition, but any execution beyond two dimensions (*e.g.*, Z stack, multichannel, and tile scanning) requires NIS Elements AR©, which costs thousands of dollars more than the BR© version (Fig. S2). PRISMS is compatible with both versions.

In general, for widefield and confocal imaging, the user will set *ZYX* coordinates and save them as either XML or CSV files, respectively. The coordinates will be interpreted as either 1) boundary points (*e.g.*, large tile scans) or 2) multipoint coordinates (*e.g.*, well plate) with *Y* by *X* tiles acquired at each coordinate (Fig. 2a). During acquisition, each *Z* coordinate will be updated in real time from an autofocus scan based on a custom, contrast-based autofocus algorithm (Fig. S3 and S4). Simultaneously, PRISMS will compute either 1) maximum intensity projections (MIPs) or 2) best focus TIFs for each tile for latter 2D stitching with Fiji/ImageJ.[20,21] Furthermore, if a user wishes to enhance the resolution with super resolution radial fluctuations (SRRF), there is an option to acquire repeated imaging and reconstruct the super resolution image (Fig. 2b).[1] We have demonstrated this tool on imaging of umbilical cord-derived mesenchymal stem cells (UC-MSCs) labeled with HSP60 and Tom20 immunofluorescence antibodies to better resolve the subcellular, mitochondrial features. Additionally, PRISMS will stitch 2D and 3D images using Fiji.[20,21] For multipoint well plate scans on a confocal microscope, we implement 3D stitching for larger depth samples with Fiji (Fig. 3).[20] Final 3D volumes are output as discrete TIF z-stacks per channel.

PRISMS enables rapid 2D and 3D stitching with single cell segmentation and quantification

Representative, multiplex IF images from human adult tonsil under Nikon widefield and Squid confocal are shown in Fig. 4a with Pan cyto-keratin (green), Ki67 (magenta), and CD4 (yellow). Corresponding single-cell masks in the bottom row were segmented by Cellpose.[22] Furthermore, PRISMS performs single-cell colocalization metrics among all pairwise markers and quantifies single-cell expression (Fig. 4b). For benchmarking, we manually stained another tonsil tissue with the same panel (Fig. S5). Similarly, representative, multiplex HCR images from another human adult tonsil slide under Squid confocal are shown in Fig. 5a with GAPDH RNA (green) and Ki67 RNA (magenta). Corresponding single-cell masks in the bottom row were segmented by Cellpose.[22] Furthermore, PRISMS performs single-cell colocalization metrics among all pairwise markers and quantifies single-cell expression (Fig. 5b).

Larger, whole tissue scans of a mouse liver fibrotic sample that was multiplexed with IF manually with 5-hmC (green), 5-mC (magenta), αSMA (white), collagen I (red), Pan cyto-keratin (cyan), and fibronectin (yellow) antibodies (Fig. 6a). Below the large area is the zoomed in region of the same tissue. Additionally, single-cell masks were drawn by Cellpose.[22] Pairwise Pearson's colocalization among all markers is shown in the bottom right boxplot. Below the diffraction limit, PRISMS can localize single mRNA molecules from HCR RNA FISH v3.0 (Fig. 6b). An example of this is shown in 01-3T3 fibroblasts multiplexed with p65 RNA and GAPDH RNA after imaging the p65 Protein reporter. The white border shows cells segmented by Cellpose.[22] Single-cell RNA counts are shown in the bottom right boxplot. Later, we multiplexed protein stainings and performed single-cell Pearson's colocalization for cells stimulated at various timepoints (Fig. S6). Together, this data highlights the spatial multi-omics capability of PRISMS.

Confocal LED matrix generates brightfield and darkfield color images with a high-sensitivity monochrome camera

Beyond fluorescence capabilities, PRISMS on confocal provides 3D fluorescence and brightfield capabilities, thus facilitating endpoint H&E for the same tissue. To demonstrate this colorimetric ability, we stained non-fibrotic and fibrotic mouse liver samples obtained from the Emory National Primate Center with Masson's Trichrome and H&E (Fig. 7). Fig. 7a shows both samples imaged with Squid confocal brightfield matrix, which is also capable of 3D RGB scanning. Meanwhile, Fig. 7b shows the same samples imaged with the

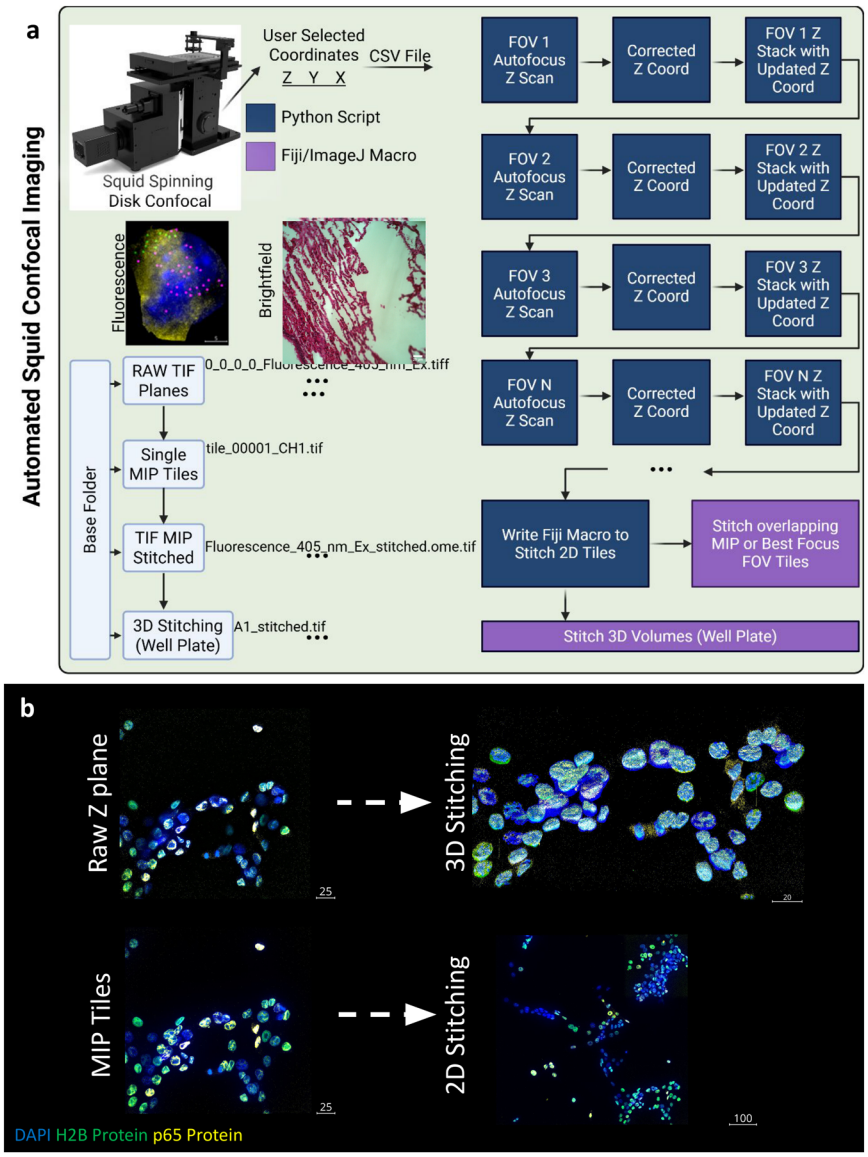

Fig. 3 PRISMS spinning disk confocal imaging pipeline. a) Main PRISMS imaging confocal acquisition workflow. Samples can be scanned with Z stack and selected fluorescent channels for multiple fields of view (FOVs), contiguous FOVs for stitching, or a combination of both in which each FOV comprises its contiguous scan, *e.g.*, 3 × 3 tiles. Regardless, each FOV is first Z-scanned on a focus channel, typically DAPI, paused for Python to compute the focus *Z* coordinate, updated in Nikon macros with the computed *Z* coordinate, and finally acquired with *Z* and channel filters. This process is repeated until all FOVs are acquired. If stitching a region defined by a boundary, Python will write a Fiji macro that can be run to stitch overlapping FOVs. Each segment of the workflow is colored by the respective programming language: Python/Jupyter (dark blue), Nikon (red), or Fiji (purple). For faster processing, tiles for stitching are computed in real time as images are acquired. Example folder structure for a single acquisition is shown in the bottom left diagram. The included brightfield LED matrix and high-sensitivity monochrome camera enable both grayscale (single-molecule) fluorescence and RGB image capabilities. Created with **BioRender.com**. b) Examples of raw and processed tiles for stitching. PRISMS confocal can stitch in 2D and 3D, with examples shown in the right column for mouse fibroblast 01-3T3 cells. DAPI (blue), H2B protein (green), and p65 protein (yellow) reporters are illustrated for these cells.

MoticEasyScan One Slide Scanner for comparison. Blue areas (collagen) indicate higher fibrotic regions. Corresponding zoomed-in regions are shown on all panels with scale bars on the bottom left or right of each.

Conclusion

Our work highlights the promise of an open-sourced, automated workflow designed for spatial omics multiplexing (Fig. 8). First, samples on slides (up to 12) are stained by an OT-2 robot in a thermal chamber with multiplex IF (protein) or HCR (RNA). Both widefield and confocal imaging platforms accommodate a wide variety of sample formats, including, but not limited to, slides, coverslips, well plates, *etc.* Samples can be readily imaged on either widefield or confocal in an automated fashion with minimal user input. The imaging pipeline includes automated fluorescence capture, SRRF reconstruction, pseudo RGB, 2D stitching, 3D stitching, single molecule localization,

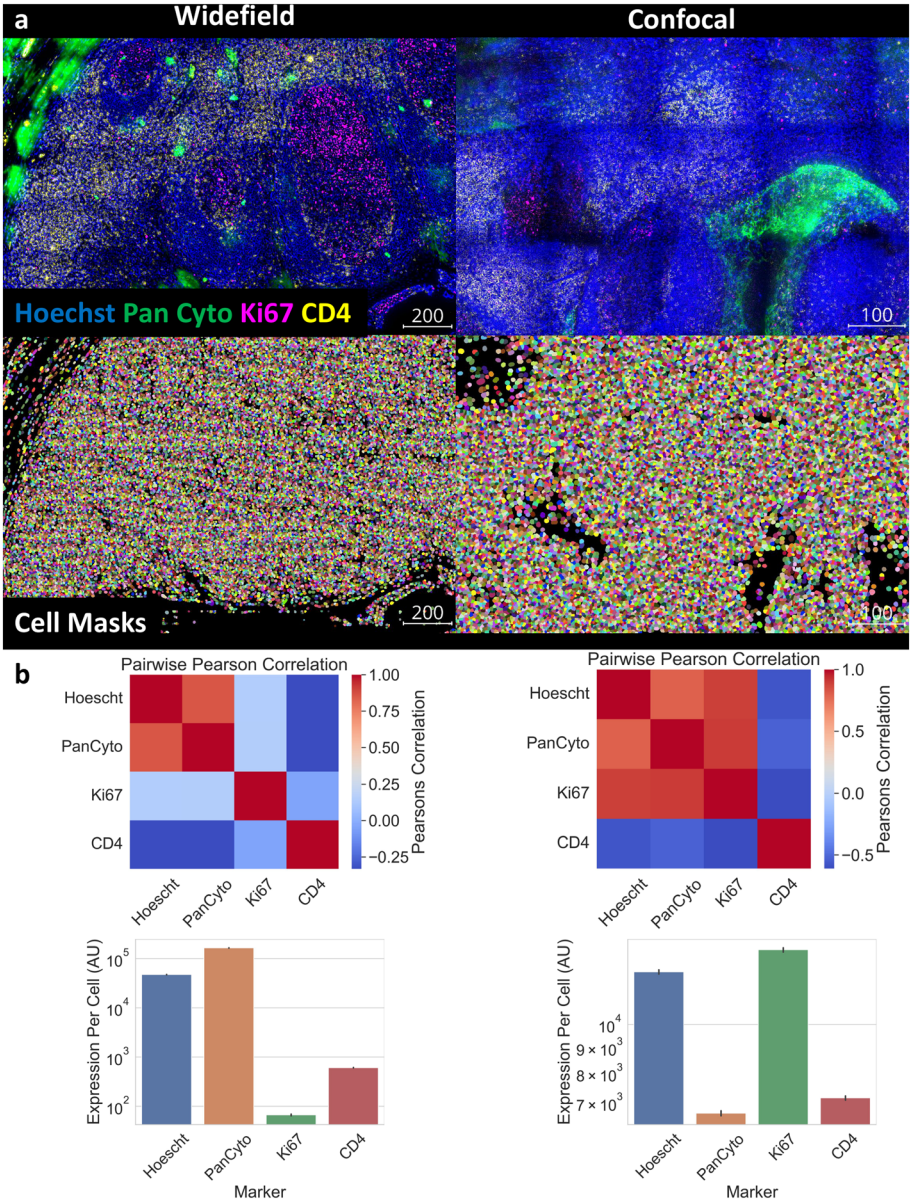

Fig. 4 Automated, multiplex immunofluorescence staining and imaging on widefield and confocal. a) Representative widefield (left column) and confocal (right column) images from automated, multiplex (2 cycles) IF staining with PRISMS on normal, adult human tonsil tissues. The scale bar is shown in white font on the bottom right. IF antibodies stained by the OT-2 robot were Hoechst (blue), pan cytokeratin (green), Ki67 (magenta), and CD4 (yellow). The bottom row illustrates the single-cell masks segmented by Cellpose.[22] b) Single-cell expression quantification comparisons between widefield and confocal. The top row shows the single-cell Pearson's correlation among all pairs of protein markers. Low colocalization is colored blue, and high colocalization is red. The bottom row quantifies the expression per cell as measured by arbitrary fluorescence intensity units.

single cell segmentation, and single cell quantification. PRISMS integrates readily available hardware and customizable software tools to streamline sample processing, thereby lowering both the financial and technical barriers to entry. By adopting an open-sourced framework, our approach not only fosters greater collaboration and transparency within the scientific community but also provides a scalable method that can be readily adapted and optimized for diverse research applications. In doing so, we aim to democratize spatial omics and empower a wider range of laboratories to contribute to this rapidly evolving field.

Materials and methods

Robotic staining, widefield, and confocal imaging

The OT-2 staining robot with a cold slim plate thermal module was obtained from Parhelia Biosciences©. The Omnistainer S12 with thermal sheath was used to stain multiple slides. For imaging, we used a Nikon TE-2000 U dissection microscope and Cephla© Squid spinning disk confocal. PRISMS Python scripts run locally on each machine and process images in real time. Both microscopes used fluorescence excitation/emission

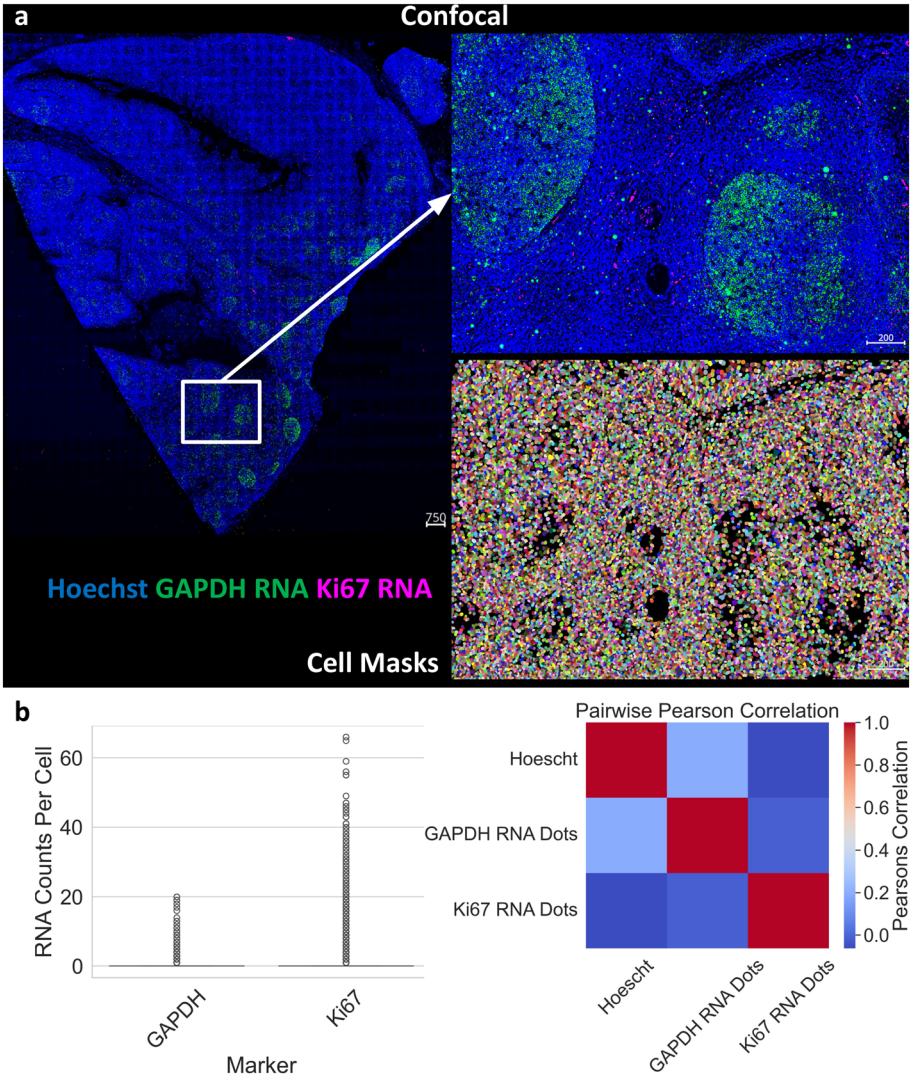

Fig. 5 Automated, multiplex RNA staining and imaging on a confocal. a) Representative confocal images from automated, multiplex (2 cycles) HCR RNA staining with PRISMS on normal, adult human tonsil tissues. The scale bar is shown in white font on the bottom right. RNA labels stained by the OT-2 robot were GAPDH RNA (magenta) and Ki67 RNA (green). Counterstained Hoechst is shown in blue. The bottom row illustrates the single-cell masks segmented by Cellpose.[22] b) Single-cell expression quantification from Squid confocal imaging of RNA. The left plot quantifies the expression per cell as measured by mRNA transcript counts per cell. The right plot shows the single-cell Pearson's correlation among RNA marker pairs. Low colocalization is colored blue, and high colocalization is red.

capabilities with appropriate filters. Additionally, the Squid confocal used an overhead LED matrix capable of emitting red, green, and blue light to create a pseudo RGB reconstruction.

Human adult tonsil samples

Formalin-fixed paraffin-embedded (FFPE) tissue slides from normal adult humans were purchased from Tissue Array, LLC. Slides were baked for 1 h at 60 °C, dewaxed, and underwent antigen retrieval with citrate buffer (pH 6) in a pressure cooker for 15 min. Then, slides were put in the Omnistainer S12 for HCR RNA FISH v3.0 or IF staining by the OT-2 robot.[18] For HCR RNA FISH v3.0, RNA probes were hybridized overnight at 37 °C using the robot thermal module. Probes were amplified in a semi-automated manner with manual user snap cooling of the hairpins at 95 °C for 90 s during robot pre-amplification. For IF, slides were incubated in antibody solution overnight at 4 °C. HCR stainings were imaged with a custom antifade bleaching buffer: 70% Tris-HCl, Trolox, 10% 1/100 catalase, 10% Pyox, and 10% of 8% glucose.

Mouse liver fibrosis samples

Formalin-fixed paraffin-embedded (FFPE) tissue slides were obtained from the Emory National Primate Center, courtesy of Dr. Arash Grakoui. BALB/c mice were either Mdr2−/− (fibrotic) or control (non-fibrotic). Slides were baked for 1 hour at 60 °C, dewaxed, and underwent antigen retrieval with citrate buffer (pH 6) in a pressure cooker for 15 min. The multiplex IF panel included 5-hmC (Active Motif 39770,

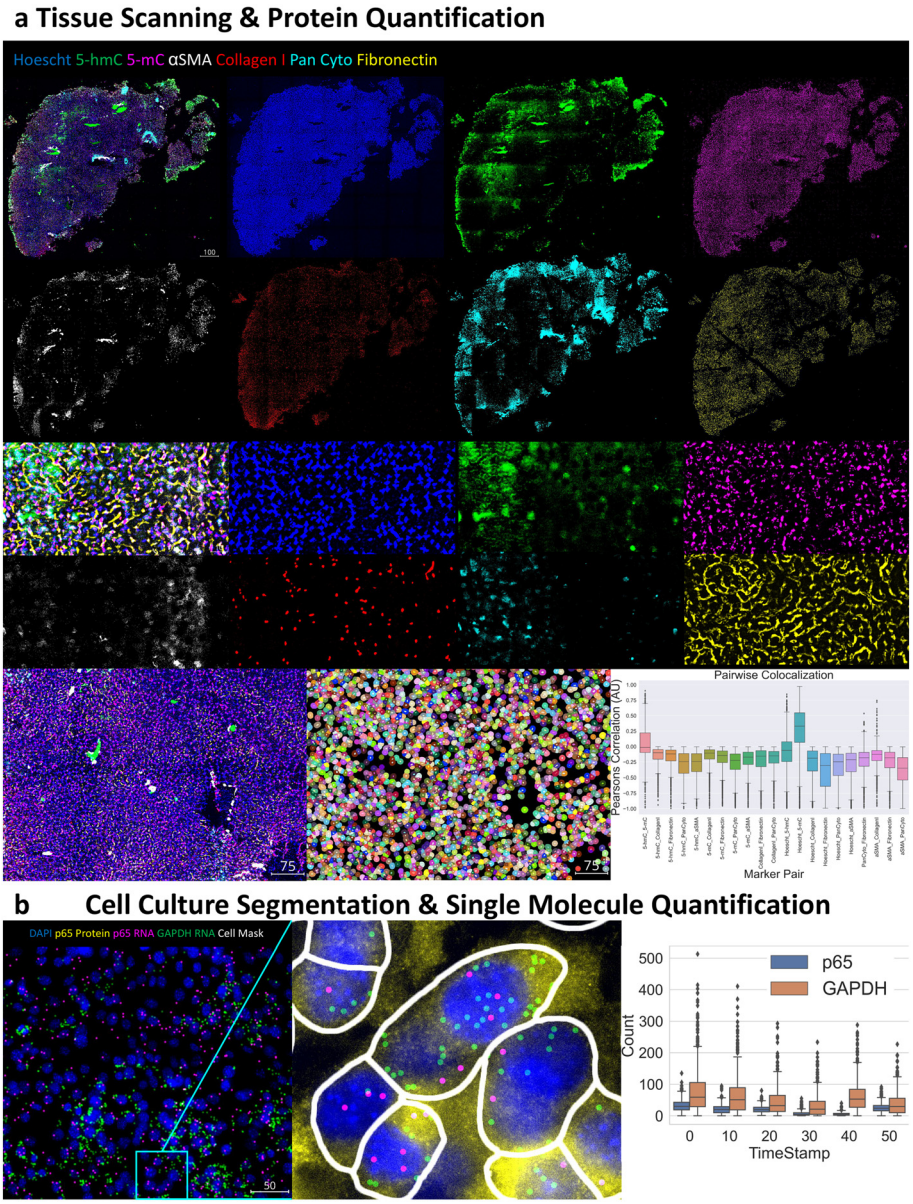

Fig. 6 PRISMS is capable of large tissue tile scans and single-molecule localization with automated single cell quantifications. a) Example of mouse liver tissue epigenetic model that was sequentially multiplexed by PRISMS. Proteomic labelling included Hoescht (blue), 5-hmC (green), αSMA (white), collagen I (red), Pan cytokeratin (cyan), and fibronectin (yellow). A whole tissue scan is shown with all markers overlaid in the top left corner and individual markers colored in neighboring panels. PRISMS automatically segments cell nuclei and cytosol with Cellpose, with each unique cell shown by a different color.[22] Single cell, spatial Pearson's correlation for each protein pair colocalization is shown in the boxplot on the bottom right.[24] b) Example of cell quantification for mouse 01-3T3 fibroblasts. p65 RNA (magenta) and GAPDH RNA (green) transcripts were multiplexed with DAPI (blue) and p65 protein (yellow). After cell segmentation (white lines), PRISMS performs localized dot counting to quantify transcript expression per cell, as shown in the boxplot on the right.

1 : 1000), 5-mC (Active Motif 39649, 1 : 500), aSMA 488 (Invitrogen 53-9760-80, 1 : 500), collagen I 647 (Abcam ab280968, 1 : 500), Pan Cyto 488 (Invitrogen 53-9003-82, 1 : 1000), and fibronectin 647 (Abcam ab237287, 1 : 500). All antibody incubations were performed overnight at 4 °C in the dark. Samples were counterstained with Hoechst and bleached with LiBH4 (1 mg mL^{-1}) for 15 min in the presence of white light after each cycle. For brightfield RGB imaging, separate samples were stained with Masson's Trichrome and H&E.

Mouse 01-3T3 fibroblast cell culture and multiplex HCR

01-3T3 mouse fibroblasts containing H2B-GFP and p65 Protein RFP reporters were obtained from Dr. Savas Tay at the University of Chicago.[23] The cell population was expanded on a T-75 flask until 70–80% confluent. Cells were stimulated with TNFα at 10 ng mL^{-1} for 10 minutes and fixed with 4% formaldehyde. To detect single-molecule RNA targets, we utilized the Molecular Instruments RNA FISH on mammalian cells on slides protocol for HCR RNA FISH v3.0. p65 protein

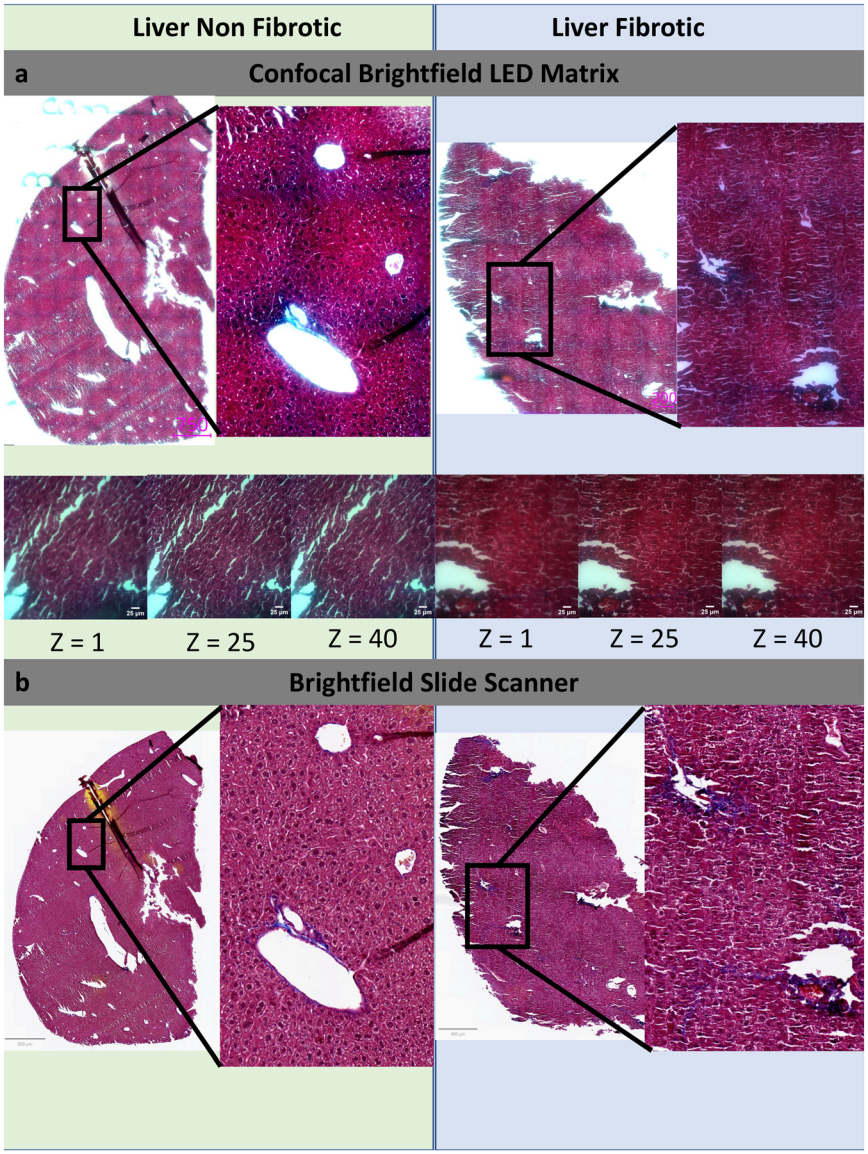

Fig. 7 PRISMS confocal enables RGB color reconstructions with a high-sensitivity monochrome camera. a) Example of mouse liver models of fibrosis. The non-fibrotic sample is shown in the left column. The fibrotic sample is shown in the right column. Both samples were stained with Masson's trichrome and imaged with PRISMS spinning disk confocal in 3D. Whole tissue scan is observed in the top row, with zoomed-in regions shown in the bottom row. H&E patterns are observed with blue denoting high collagen (fibrotic) regions. Confocal enables 3D Z scanning of each tile (bottom row). b) Same tissues in (a) imaged with the Motic slide scanner for reference. Whole tissue scan is observed in the left part, with zoomed-in regions shown in the right part. H&E patterns are observed with blue denoting high collagen (fibrotic) regions.

and H2B-protein reporters were imaged in the first cycle after only formaldehyde fixation. p65 protein was imaged in the ds-RED/TRITC channel, and H2B protein was imaged in the A488/GFP channel. Then, samples were permeabilized in 70% ethanol at −20 °C for 30 min. HCR probes were detected in HCR probe hybridization buffer, amplified overnight in HCR amplification buffer, and washed with 5X SSC. HCR stainings were imaged with a custom antifade bleaching buffer: 70% Tris-HCl, Trolox, 10% 1/100 catalase, 10% Pyox, and 10% of 8% glucose.

For multiplexing to gain multi-omics data, due to the unavailability of GFP and TRITC channels due to existing H2B and p65 protein reporter signals, respectively, we only used the Alexa Fluor 647 fluorescent channel for HCR detection using B1 amplifiers. To multiplex p65 RNA and GAPDH RNA, we performed the first detection of p65 RNA in the Alexa Fluor 647 channel, and then digestion of HCR assembly using DNase I enzyme for 4 h at room temperature. In the subsequent cycle, we performed GAPDH RNA detection using the same Alexa Fluor 647 channel as a positive control. GAPDH RNA signal was removed with DNase I again for 4 h at RT. Later, A20 Ab was labeled overnight, imaged, and quenched with DNAse and LiBH4 (1 mg ml^{-1}) bleach for 15 min under white light. Finally, segmentation of Abs (Vim, Hsp47, S100A4, and αSMA) was labeled in the final cycle for later 3D cell segmentation. We performed image

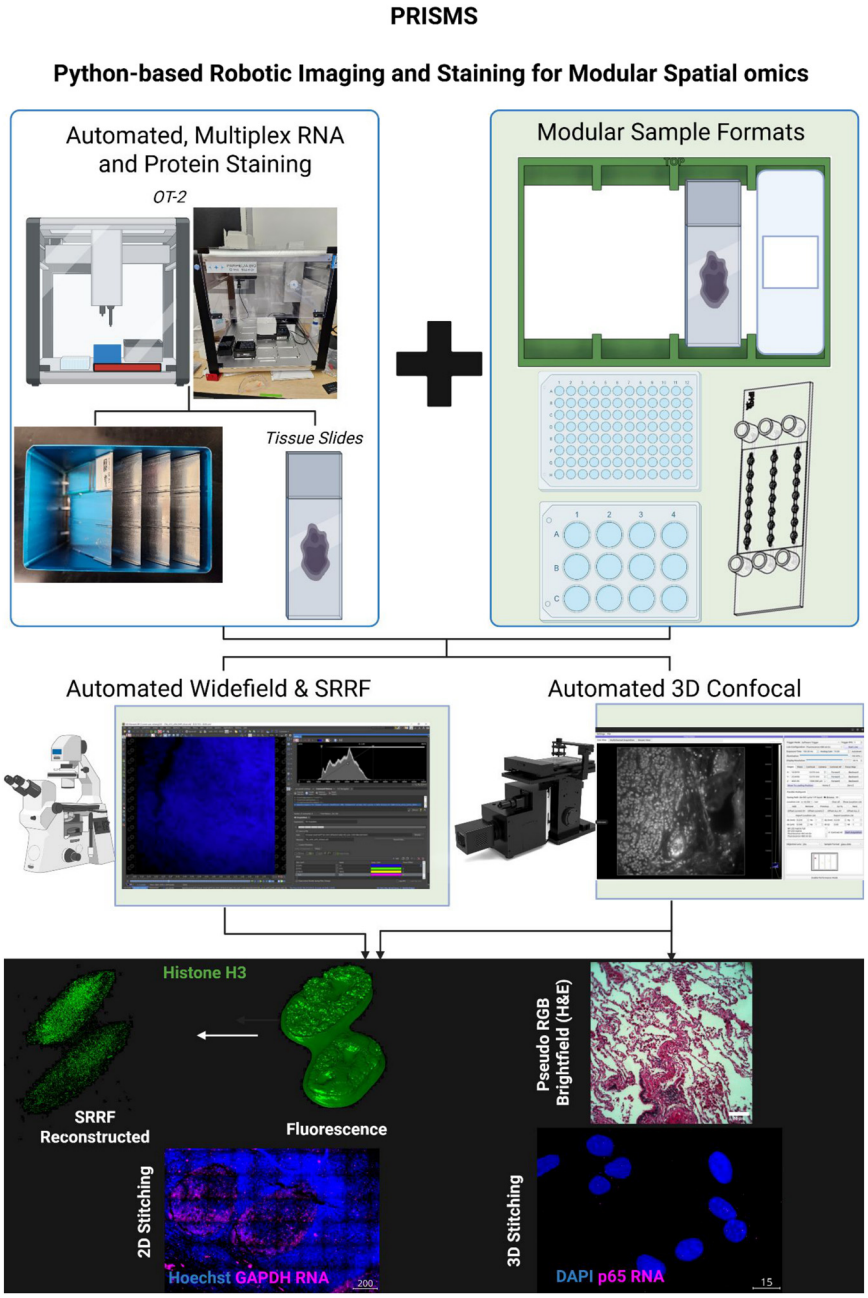

Fig. 8 Summary of PRISMS workflow. The top left panel shows the automated spatial transcriptomic and proteomics labeling capabilities with the OT-2 robot. Samples can be multiplexed in high throughput using a thermal module for heating and cooling steps. The top right panel illustrates the sample format variety that PRISMS is capable of imaging, ranging from custom 3D printed slide/coverslip mounts (green) to standard well plate formats to custom Ibidi microchannels. Next, samples can be imaged on either an automated Nikon widefield or Cephla© spinning disk confocal (middle row). Widefield images can be repeatedly acquired to generate an SRRF super-resolved reconstruction.[1] 3D confocal images can either be fluorescence or artificial color images with the aid of an LED matrix coupled with a high-sensitivity monochrome camera. The left bottom row shows an example of SRRF reconstruction applied to 2 mesenchymal stem cells labeled with Histone H3 antibody (green). The right bottom row shows an example confocal RGB of human lung tissue H&E. The last row shows examples of 2D stitching – human adult tonsil with GAPDH RNA – and 3D stitching – 01-3T3 fibroblasts with p65 RNA. All scale bars are denoted in white. Created with **BioRender.com**.

registration across cycles using nuclear signatures from reporter protein imaging, p65 RNA, and GAPDH RNA imaging cycles. After cell segmentation with Cellpose, we computed single-cell Pearson's colocalization among all pairwise markers, thus demonstrating the multi-omics capability of PRISMS (Fig. S6).

Z-stack autofocus algorithm

Our algorithm is designed to determine the focus plane in a 3D image stack (a series of 2D images along the *z*-axis) using a modified Laplacian variance method. The Laplacian variance is a measure of image sharpness, where higher variance

indicates sharper images with more edges and details. The algorithm processes each *z*-plane in the stack, computes its sharpness, and identifies the plane with the highest sharpness or focus. The algorithm begins by calculating the Laplacian variance for each *z*-plane in the stack. The Laplacian operator highlights edges and areas of rapid intensity change in an image. For each plane, the Laplacian is computed using OpenCV, and its variance is calculated. This variance serves as a measure of sharpness for the plane. To handle large datasets efficiently, the algorithm uses Dask for parallel and lazy computation. Each plane's Laplacian variance is computed as a delayed task, and the results are concatenated into a single array (lapVar) after computation. Once the Laplacian variance is calculated for all planes, the algorithm identifies the plane with the highest variance using np.argmax(lapVar). This plane is the initial candidate for the focus plane, as it is the sharpest based on the Laplacian variance. To refine the focus plane selection, the algorithm computes the gradient of the Laplacian variance array. The gradient measures how quickly the variance changes between consecutive planes, and its square is taken to emphasize larger changes. Peaks in the gradient are then identified using scipy.signal.find_peaks. These peaks represent planes where the sharpness changes most steeply, which could indicate transitions to focused planes. If no peaks are found in the gradient, the algorithm defaults to the middle plane of the stack as the focus plane. Otherwise, it selects the first peak as the focus plane, with adjustments to ensure the selected plane does not exceed the bounds of the stack. This ensures robustness in cases where the gradient analysis might fail to detect clear peaks.

2D and 3D stitching

For 2D stitching, each tile is computed based on the best focus (computed *via* the autofocus algorithm) or maximum intensity projection. Then, PRISMS writes a Fiji macro to stitch the tiles *via* MIST.[21] We perform 2D stitching with the following parameters: blendingmode = LINEAR, blendingalpha = 1.5, compressionmode = UNCOMPRESSED, numcputhreads = 32, loadfftwplan = true, savefftwplan = true, fftwplantype = MEASURE, fftwlibraryname = libfftw3, fftwlibraryfilename = libfftw3.dll, stagerepeatability = 0, horizontaloverlap = 15.0 (%), verticaloverlap = 15.0 (%), numfftpeaks = 0, overlapuncertainty = NaN, isusedoubleprecision = false isusebioformats = false, issuppressmodelwarningdialog = true, isenablecudaexceptions = false, translationrefinementmethod = SINGLE_HILL_CLIMB, numtranslationrefinementstartpoints = 16, headless = false, loglevel = MANDATORY, debuglevel = NONE.

For 3D stitching, typically for well plates, additional 3D stitching is performed *via* Fiji macros executed on raw 3D tiles of ZYX dimension.[20] 3D stitching would be performed for 3–5 tiles along each dimension. To accomplish this in Fiji, we implemented the following parameters: tile_overlap = 15 (%), fusion_method = [Linear Blending], regression_threshold = 0.30, max/avg_displacement_threshold = 2.50, absolute_displacement_threshold = 3.50, computation_parameters = [Save memory (but be slower)], image_output = [Write to disk].

Conflicts of interest

A. F. C. and N. Z. declare a patent application related to the automated spatial omics platform (US Provisional 63/810,342). The other authors declare no competing interests.

Data availability

Supplementary information: The SI contains more technical details, validations, and comparisons to other spatial omics platforms. See DOI: **https://doi.org/10.1039/D5LC00286A**.

The data and pipeline that support the findings of this study are openly available in Figshare and GitHub.

https://figshare.com/articles/dataset/Modular_Open-Sourced_Multiplexing_for_Democratizing_Spatial_Multi-Omics/28646996.

https://github.com/coskunlab/PRISMS.

Acknowledgements

A. F. C. holds a career award at the Scientific Interface from the Burroughs Wellcome Fund and a Bernie–Marcus Early-Career Professorship. A. F. C. was supported by start-up funds from the Georgia Institute of Technology and Emory University. Research reported in this study was partially supported by the NSF CAREER under award number 2338935, National Institutes of Health under award numbers R35GM151028, T32GM142616, and 1R21AI173900.

References

1 N. Gustafsson, S. Culley, G. Ashdown, D. M. Owen, P. M. Pereira and R. Henriques, *Nat. Commun.*, 2016, **7**, 12471.
2 Q. Blampey, K. Mulder, C.-A. Dutertre, M. Gardet, F. André, F. Ginhoux and P.-H. Cournède, *bioRxiv*, 2023, preprint, DOI: **10.1101/2023.12.22.571863**.
3 R. Henley, N. Rapicavoli, A. Janesick, R. Shelansky, A. Kim, J. Hensel, F. Meschi, N. Farahani, V. Kumar, X. Qian and S. Taylor, *J. ImmunoTher. Cancer*, 2022, **10**, DOI: **10.1136/jitc-2022-SITC2022.0095**.
4 G. Emanuel and J. He, *Microsc. Today*, 2021, **29**, 16–19.
5 Z. R. Lewis, T. Phan-Everson, G. Geiss, M. Korukonda, R. Bhatt, C. Brown, D. Dunaway, J. Phan, A. Rosenbloom, B. Filanoski, R. Meredith, K. Chantranuvatana, Y. Liang, E. Brown, B. Birditt, G. Ong, H. S. Yi, E. Piazza, V. Devgan, N. Ortogero, P. Danaher, S. Warren, M. Rhodes and J. Beechem, *Cancer Res.*, 2022, **82**, 3878.
6 A. Kinkhabwala, C. Herbel, J. Pankratz, D. A. Yushchenko, S. Rüberg, P. Praveen, S. Reiß, F. C. Rodriguez, D. Schäfer, J. Kollet, V. Dittmer, M. Martinez-Osuna, L. Minnerup, C. Reinhard, A. Dzionek, T. D. Rockel, S. Borbe, M. Büscher, J. Krieg, M. Nederlof, M. Jungblut, D. Eckardt, O. Hardt, C. Dose, E. Schumann, R.-P. Peters, S. Miltenyi, J. Schmitz, W. Müller and A. Bosio, *Sci. Rep.*, 2022, **12**, 1911.

7 M. J. Abraham, C. Goncalves, P. McCallum, V. Gupta, S. E. J. Preston, F. Huang, H. Chou, N. Gagnon, N. A. Johnson, W. H. Miller, K. K. Mann and S. V. del Rincon, *Cell Biosci.*, 2024, **14**, 19.
8 T. R. Sztanka-Toth, M. Jens, N. Karaiskos and N. Rajewsky, *GigaScience*, 2022, **11**, giac064.
9 J. F. Navarro, J. Sjöstrand, F. Salmén, J. Lundeberg and P. L. Ståhl, *Bioinformatics*, 2017, **33**, 2591–2593.
10 G. Palla, H. Spitzer, M. Klein, D. Fischer, A. C. Schaar, L. B. Kuemmerle, S. Rybakov, I. L. Ibarra, O. Holmberg, I. Virshup, M. Lotfollahi, S. Richter and F. J. Theis, *Nat. Methods*, 2022, **19**, 171–178.
11 F. Curion, C. Rich-Griffin, D. Agarwal, S. Ouologuem, K. Rue-Albrecht, L. May, G. E. L. Garcia, L. Heumos, T. Thomas, W. Lason, D. Sims, F. J. Theis and C. A. Dendrou, *Genome Biol.*, 2024, **25**, 181.
12 L. Pollaris, B. Vanneste, B. Rombaut, A. Defauw, F. Vernaillen, J. Mortier, W. Vanhenden, L. Martens, T. Thoné, J.-F. Hastir, A. Bujko, W. Saelens, J.-C. Marine, H. Nelissen, E. V. Hamme, R. Seurinck, C. L. Scott, M. Guilliams and Y. Saeys, *bioRxiv*, 2024, preprint, DOI: **10.1101/2024.07.04.601829**.
13 C. Xia, J. Fan, G. Emanuel, J. Hao and X. Zhuang, *Proc. Natl. Acad. Sci. U. S. A.*, 2019, **116**, 19490–19499.
14 M. Schott, D. León-Periñán, E. Splendiani, L. Strenger, J. R. Licha, T. M. Pentimalli, S. Schallenberg, J. Alles, S. S. Tagliaferro, A. Boltengagen, S. Ehrig, S. Abbiati, S. Dommerich, M. Pagani, E. Ferretti, G. Macino, N. Karaiskos and N. Rajewsky, *Cell*, 2024, **187**, 3953–3972.e26.
15 J. De Jonghe, J. W. Opzoomer, A. Vilas-Zornoza, B. S. Nilges, P. Crane, M. Vicari, H. Lee, D. Lara-Astiaso, T. Gross, J. Morf, K. Schneider, J. Cudini, L. Ramos-Mucci, D. Mooijman, K. Tiklová, S. M. Salas, C. M. Langseth, N. D. Kashikar, E. M. Carrami, R. McIntyre, C. B. Swerner, E. M. Hessel, C.-A. Kapourani, C. Regep, C. E. S. Roberts, D. Schapiro, J. Lundeberg, M. Nilsson, A. K. Shalek, A. P. Cribbs and J. P. Taylor-King, *Cell Genomics*, 2024, **4**, 100723.
16 M. Yasui, M. Hiroshima, J. Kozuka, Y. Sako and M. Ueda, *Nat. Commun.*, 2018, **9**, 3061.
17 H. Pinkard, N. Stuurman, I. E. Ivanov, N. M. Anthony, W. Ouyang, B. Li, B. Yang, M. A. Tsuchida, B. Chhun, G. Zhang, R. Mei, M. Anderson, D. P. Shepherd, I. Hunt-Isaak, R. L. Dunn, W. Jahr, S. Kato, L. A. Royer, J. R. Thiagarajah, K. W. Eliceiri, E. Lundberg, S. B. Mehta and L. Waller, *Nat. Methods*, 2021, **18**, 226–228.
18 H. M. T. Choi, M. Schwarzkopf, M. E. Fornace, A. Acharya, G. Artavanis, J. Stegmaier, A. Cunha and N. A. Pierce, *Development*, 2018, **145**, dev165753.
19 M. Venkatesan, N. Zhang, B. Marteau, Y. Yajima, N. O. De Zarate Garcia, Z. Fang, T. Hu, S. Cai, A. Ford, H. Olszewski, A. Borst and A. F. Coskun, *Sci. Rep.*, 2023, **13**, 5374.
20 S. Preibisch, S. Saalfeld and P. Tomancak, *Bioinformatics*, 2009, **25**, 1463–1465.
21 J. Chalfoun, M. Majurski, T. Blattner, K. Bhadriraju, W. Keyrouz, P. Bajcsy and M. Brady, *Sci. Rep.*, 2017, **7**, 4988.
22 C. Stringer, T. Wang, M. Michaelos and M. Pachitariu, *Nat. Methods*, 2021, **18**, 100–106.
23 M. Son, T. Frank, T. Holst-Hansen, A. G. Wang, M. Junkin, S. S. Kashaf, A. Trusina and S. Tay, *Sci. Adv.*, 2022, **8**, eabn6240.
24 K. W. Dunn, M. M. Kamocka and J. H. McDonald, *Am. J. Physiol.*, 2011, **300**, C723–C742.